

Absolute frequency measurement of the $6P_{1/2} \rightarrow 7S_{1/2}$ transition in thalliumTzu-Ling Chen,¹ Isaac Fan,¹ Hsuan-Chen Chen,² Chang-Yi Lin,¹ Shih-En Chen,¹ Jow-Tsong Shy,^{1,2} and Yi-Wei Liu^{1,*}¹*Department of Physics, National Tsing Hua University, Hsinchu, Taiwan 30013*²*Institute of Photonics Technologies, National Tsing Hua University, Hsinchu, Taiwan 30013*

(Received 18 September 2012; published 29 November 2012)

The absolute frequency measurement of thallium $6P_{1/2} \rightarrow 7S_{1/2}$ transitions using a self-referencing optical frequency comb is reported. Our results can be used as a benchmark for the accurate wave-function calculations of heavy atoms, and then improve the calculations of the atomic parity-nonconservation amplitude. The frequency centers have been precisely determined by the Doppler-free saturation spectroscopy utilizing a pair of the counterpropagating laser beams intersecting with a thallium atomic beam. We have achieved the absolute frequency determination of the transition with an accuracy of 350 kHz. The isotope shift and hyperfine splittings are also deduced from our results. The hyperfine splittings of the $7S_{1/2}$ state are improved to sub-MHz accuracy. Meanwhile, the nuclear isotopic changes resulting from the $7S_{1/2}$ and $6P_{1/2}$ hyperfine anomalies are in agreement with earlier measurements.

DOI: [10.1103/PhysRevA.86.052524](https://doi.org/10.1103/PhysRevA.86.052524)

PACS number(s): 32.30.-r, 32.10.Fn

I. INTRODUCTION

High-precision measurements in atomic systems show a promising approach in testing the standard model (SM) of elementary particles and searching for the new physics beyond it. Various atomic systems (e.g., Cs, Tl, Yb, etc.) play important roles in atomic parity-nonconservation (PNC) and permanent electric dipole moment (EDM) experiments mainly attributed to their atomic number Z , which enlarge the PNC and EDM effects by Z^3 . In the most accurate atomic PNC experiment, 0.35% accuracy had been achieved in cesium [1]. Combining the theoretical atomic-structure calculations of 0.5% accuracy [2], it leads to a measurement of the weak charge Q_W of the cesium nucleus, which can be compared to the predication of the SM and be tested. This result is one of the most accurate low-energy tests of the electroweak sector of the SM to date. The PNC effect had also been observed in atomic thallium systems since 1995 and reached 1.7% of experimental uncertainty [3,4]. By contrast, the theoretical uncertainty for thallium is limited at the level of 2.5% [5–7] due to the complicated atomic structure. The resulting total uncertainty of the inferred Q_W of thallium nucleus is 3.0% and places a limit on the analysis and interpretation of the single-isotope PNC measurements.

In atomic thallium, there exists a strong correlation among the three valence electrons and hence it can not be treated accurately using the conventional many-body perturbation theory (MBPT), as pointed out by Kozlov [5] and Dzuba [8]. There are several theoretical approaches developed to incorporate the correlation effect, such as the improved MBPT with the configuration interaction and the coupled-cluster method [9]. To verify the accuracy of these developing MBPT methods, however, various observables such as transition energies, hyperfine splittings, transition amplitudes, and polarizabilities need to be compared with the corresponding experimental values [10].

Among the lower-lying energy levels of Tl, the $6P_{1/2} \leftrightarrow 7S_{1/2}$ transition is of particular interest. An accurate energy

determination of this ground-state transition not only can aid the development of the MBPT, but it can also complement experiments where this transition is utilized, such as in the laser cooling of Tl [11]. Hyperfine splittings and isotope shifts of this transition have been previously measured in the vapor gas cell [12] and atomic beam [13] setups. The precision in both setups, however, is mostly limited by the frequency calibration. In our experiment, the absolute frequency calibration against optical frequency comb (OFC) is a key motivation in the precision improvement. The OFC is a versatile optical frequency measuring tool with an accuracy of kHz or better. Therefore, the precision of optical transition frequency measurement is limited by the linewidth of the observed atomic or molecular transitions and the signal-to-noise ratio of the spectrum, rather than the frequency measuring tool.

The Doppler-broadened linewidth, in principle, can be eliminated using the saturation spectroscopy technique [14–16]. In such cases, the decrease (a dip) of the absorption strength on the resonance is induced by the saturation effect and the dip profile can be interpreted as Doppler free, having a linewidth close to the natural linewidth of the corresponding transition.

For Tl, the atomic beam setup should have a distinct advantage over the vapor cell setup in terms of observing the Doppler-free feature. The three $6P_{1/2} \leftrightarrow 7S_{1/2} \leftrightarrow 6P_{3/2}$ levels of Tl constitute a Λ -type energy system (Fig. 1) where the saturation intensity of the $6P_{1/2} \leftrightarrow 7S_{1/2}$ transition is significantly reduced due to the presence of the $6P_{3/2}$ metastable state [17,18], which traps the population with a long lifetime. In such a three-level Λ system, the population is easily saturated and an additional homogeneous broadening (e.g., power broadening) can be present in the signal profile. This is especially true in the vapor cell setup where the same Tl atom is likely to absorb multiple photons before it leaves the interaction region. In the atomic beam setup, on the other hand, a continuous influx of fresh Tl atoms prevents the lowering of the saturation intensity by limiting the time atoms reside in the interaction region. The tradeoff is the transit-time broadening, which is estimated to be less than 0.1 MHz if a 1-mm-sized laser beam shines onto an atomic beam with a velocity of 243 m/s.

In this paper, the saturation spectroscopy technique is applied to a Tl atomic beam to carry out a frequency comb

*ywliu@phys.nthu.edu.tw

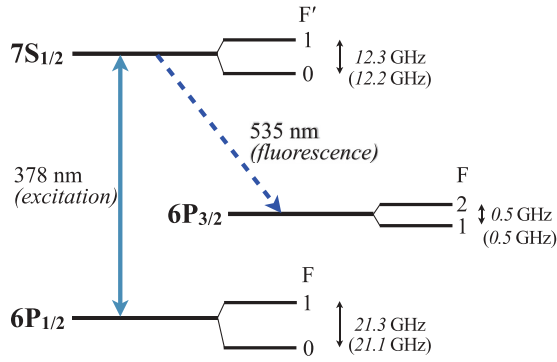


FIG. 1. (Color online) Simplified energy-level diagram of ^{205}Tl (^{203}Tl). Level shifts are not to scale.

measurement on all $6P_{1/2} \leftrightarrow 7S_{1/2}$ hyperfine transitions without the Doppler-broadening effect. The well-known saturation dip (Lamb dip) is observed and its absolute frequency is shown to be independent of the geometric relation between the optical beam (pump and probe) and the atomic beams under the condition that a *collinearity* for the counterpropagating optical beams is maintained. This removes the potential Doppler shift induced by the nonperpendicular intersection of the laser and the atomic beam, and hence alleviates a common systematic error that hinders the absolute frequency measurement in an atomic beam setup [19–22].

In addition, the absolute frequency of the $6P_{1/2} \leftrightarrow 7S_{1/2}$ transition in Tl is measured with a sub-MHz accuracy. Along with the derived hyperfine splittings and isotope shifts, these measurements should provide information for evaluating the MBPT method.

II. EXPERIMENT

The experimental setup is a typical pump-probe configuration with a thermal atomic beam. A schematic representation is shown in Fig. 2. The 378-nm laser source was generated by frequency doubling the 755-nm light from a

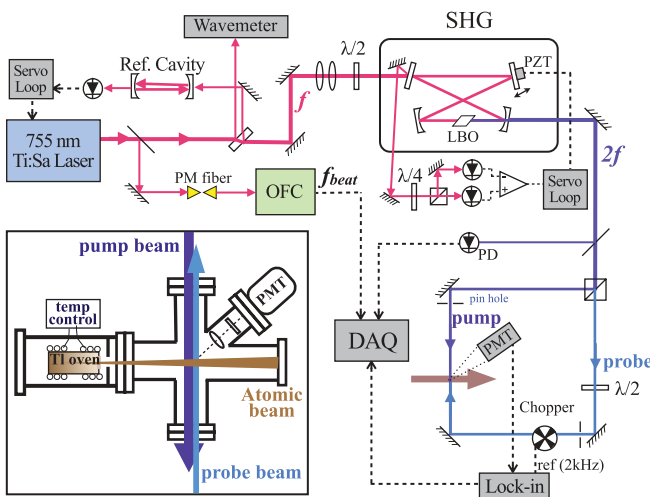


FIG. 2. (Color online) The experimental setup of the absolute frequency measurement of thallium $6P_{1/2} \rightarrow 7S_{1/2}$ transition. Inset: The atomic beam apparatus.

Ti:sapphire laser, and split into pump and probe beams in counterpropagating directions. Both of them were linearly polarized and perpendicularly intersecting with the atomic beam. To improve pumping efficiency and to take advantage of the long lifetime of the metastable $6P_{3/2}$ state, the technique of optical pumping, as [15], was employed, that is, setting the pump beam to be in front of the probe beam rather than fully overlapping each other. So, the atoms first interacted with pump beam and the population of $6P_{1/2}$ state was depleted, before probing. The probe beam intensity was modulated using an optical chopper with a frequency of 2 kHz to eliminate the background light produced by the pump beam. The laser-induced 535-nm fluorescence ($7S_{1/2} \rightarrow 6P_{3/2}$) was detected using a photomultiplier, and demodulated using a lock-in amplifier.

A. Apparatus

A power of 1–2 mW of 378-nm UV light was generated using a LBO crystal in an enhancement cavity with an X-type ring configuration. The cavity was locked to the fundamental laser frequency using the technique of polarization rotation. The detailed description of the system can be found in Ref. [11]. The UV light was then collimated to a beam size of $3 \text{ mm} \times 10 \text{ mm}$ using an AR coated lens. The elliptic beam shape was for a longer interaction time along the atomic beam propagating direction, therefore a higher pumping efficiency and a smaller transit-time broadening.

As shown in the inset of Fig. 2, the thermal atomic beam, operated in a stainless chamber with a background pressure of 10^{-5} Torr, was produced from bulk thallium heated to 450°C . It was then sieved out using two apertures with diameters of 2 and 4.35 mm separated by 12.85 mm, corresponding to a divergence of 90 mrad. The most probable velocity of thallium atoms was $\sim 243 \text{ m/s}$. The density of atoms in the beam was $\sim 10^{12} \text{ cm}^{-3}$.

The 755-nm fundamental laser pumped by a 7-W 532-nm laser provided a power of $\sim 850 \text{ mW}$, and was locked to a reference cavity with a finesse of 310 and a free spectral range of 1.07 GHz. This cavity was also equipped with a piezostack for frequency scanning. The frequency jitter was then reduced to $< 0.1 \text{ MHz}$ within 0.1 s, and the observed frequency drift over 15 min was $< 15 \text{ kHz/s}$ due to the ambient temperature change.

B. Spectrum and frequency measurement

For the absolute frequency calibration, a part of the 755-nm laser output was mixed with the OFC radiation. The detailed information of the OFC system we used can be found in [23]. The 755-nm laser delivered to the OFC was through a polarization-maintaining fiber to avoid the fluctuation of the laser power due to the birefringence of optical fiber. The 755-nm laser and the OFC were then combined using a polarizing beam splitter and their beat frequency (f_{beat}), which was detected using an avalanche photodiode and measured using a counter. For a reliable counting of the beat frequency, the signal of beat note was kept to be $> 30 \text{ dB}$ above the noise level.

The scan rate of the 755-nm laser was 30 MHz/min . A single scan consisted of 1000–1500 data points within the

frequency range of 300 MHz in terms of the 755-nm laser frequency. Each data point was a set of information including the beat frequency f_{beat} , OFC repetition rate f_{rep} , OFC offset frequency f_o , the averaged fluorescence signal amplitude, the standard deviation of the fluorescence signal, and the 378-nm laser power. The data collecting rate was 2 sets/s. The time constant of the lock-in amplifier was 30 ms, which was sufficiently short to follow such a slow scan rate. Furthermore, during data taking, two frequency upward and downward scans (four scans) were performed to cancel out any possible “scan direction-dependent” systematic effect.

C. Lineshape model

A typical lineshape of the saturation dip with a Doppler-broadened background is a Lorentzian dip on the top of a Gaussian profile. However, it would be insufficient to fully describe our experimental observations, which are composed of the homogeneous and the inhomogeneous broadening effects with dispersive asymmetry. To incorporate these features, in our experiment, the lineshape model is

$$S(\omega) = [\alpha + A(\omega, \omega_0 + \omega_{\text{shift}})]V(\omega, \omega_0 + \omega_{\text{shift}}, \Gamma_{L1}, \Gamma_G) - \beta L(\omega, \omega_0, \Gamma_{L2}) + c, \quad (1)$$

where Γ_{L1} and Γ_{L2} are the linewidths of the Lorentzian (homogeneous) profiles of the probe and pump, Γ_G is the Gaussian width including Doppler and inhomogeneous broadening, ω_0 is the center frequency of the transition, and ω_{shift} is a small value that describes the frequency shift between the Voigt background and the Lorentzian dip due to imperfect perpendicularity between the atomic beam and the lasers.

The first term in Eq. (1) is the Doppler-broadened background with an asymmetrical profile. The second term is the Doppler-free dip. The Voigt function $V(\omega, \omega_0 + \omega_{\text{shift}}, \Gamma_{L1}, \Gamma_G)$ is the convolution of the Gaussian and Lorentzian functions to describe the mixing of the homogeneous-inhomogeneous broadening. The Lorentzian function $L(\omega, \omega_0, \Gamma_{L2})$ is the homogeneously broadened, Doppler-free dip. The minus sign of the second term indicates the “dip.”

$A(\omega, \omega_0 + \omega_{\text{shift}})$ is a derivative Gaussian profile for the asymmetry of the background profile. The asymmetric feature has been observed in many spectroscopy experiments using the fluorescence or absorption techniques, and found to be induced by various mechanisms, including the atomic recoil effect in a dispersive medium [24], velocity-dependent collision time effect [25], as well as the atomic recoil effect due to the velocity-dependent force in the traveling-wave case [26]. The degree of the lineshape asymmetry can be quantified using a single parameter ϵ , the ratio of the maximum slopes of the two sides of the peak, as defined by [26]. The value of ϵ is ~ 0.85 in our work. For a small asymmetry, a derivative Gaussian profile is a good approximation [27]:

$$\begin{aligned} A(\omega, \omega_0 + \omega_{\text{shift}}) &= \frac{d}{d\omega} \text{Gaussian}(\omega, \omega_0 + \omega_{\text{shift}}, \Gamma) \\ &= a[\omega - (\omega_0 + \omega_{\text{shift}})] \text{Gaussian}(\omega, \omega_0 + \omega_{\text{shift}}, \Gamma). \end{aligned} \quad (2)$$

This model works well with our experimental results, as the fitting residuals show mostly random noise without any

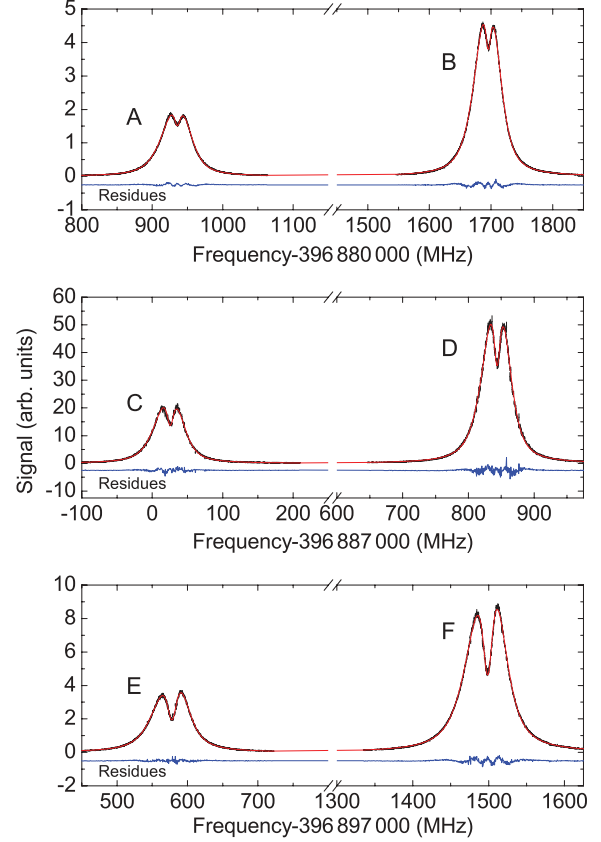


FIG. 3. (Color online) The spectrum of all hyperfine transitions. The fitting line (red solid curve) and fitting residues (blue curve) are also shown. The frequency axis shown in this figure is the frequency of the fundamental 755-nm laser. A: $[^{203}\text{Tl}] 6P_{1/2}(F=1) \rightarrow 7S_{1/2}(F'=0)$, B: $[^{205}\text{Tl}] 6P_{1/2}(F=1) \rightarrow 7S_{1/2}(F'=0)$, C: $[^{203}\text{Tl}] 6P_{1/2}(F=1) \rightarrow 7S_{1/2}(F'=1)$, D: $[^{205}\text{Tl}] 6P_{1/2}(F=1) \rightarrow 7S_{1/2}(F'=1)$, E: $[^{203}\text{Tl}] 6P_{1/2}(F=0) \rightarrow 7S_{1/2}(F'=1)$, F: $[^{205}\text{Tl}] 6P_{1/2}(F=0) \rightarrow 7S_{1/2}(F'=1)$.

special pattern (see Fig. 3). The ratio of asymmetry of our spectrum fitted to this model is $(a/\alpha) < 2\%$. The fitting program was written on ROOT platform (CERN) using the built-in Voigt function.

III. RESULTS AND DISCUSSION

A. Doppler-free spectrum

Figure 3 shows all the hyperfine transitions of $6P_{1/2} \rightarrow 7S_{1/2}$ in Tl with the fitting curves and the residues. Each spectrum is a histogram composed of four individual scans with a 500-kHz bin size, which was chosen to be efficient and without losing any accuracy. The error bars of the histogram were given by the deviation of the fluorescence signal strength within the same laser frequency bin. The signal-to-noise ratio (SNR) is 35–50, which allows a sub-MHz accuracy in measuring the center frequency of a dip with a 13 to 20 MHz width.

The dip widths of $6P_{1/2}(F=1) \rightarrow 7S_{1/2}(F'=0)$ (A and B) are only ~ 13 MHz and smaller than the other hyperfine transitions to the $F'=1$ excited states, which are C, D, E, and F lines with dip widths ~ 20 MHz. This is due to a larger

TABLE I. Budget of uncertainties of absolute transition frequency in $6P_{1/2} \rightarrow 7S_{1/2}$ measured on a thermal atomic beam: statistical results and systematic error budget. All the values are in MHz.

Source	Uncertainties (MHz)
Statistics	0.22
Frequency comb	0.04
Residue Doppler shift	0.27
Second-order Doppler	0.0003
Zeeman effect	0.01
Total	0.35

branching decay rate of $7S_{1/2}(F' = 1)$ to the metastable $6P_{3/2}$ state, which causes a lower effective saturation intensity and a stronger power broadening. The widths of the background Voigt profiles are 30–50 MHz contributed from the natural linewidth (5–16 MHz), the first-order Doppler broadening, and the power broadening. All of the laser linewidth (0.1 MHz with 0.1-s integration time [23]), the transit-time broadening (<0.01 MHz), and the collision broadening (<0.1 MHz) are negligible in our experiment.

B. Frequency uncertainty assessment

The frequency uncertainties contributed from the various sources, including the statistical and the systematic, are summarized in Table I. The statistical uncertainty of the center frequency is from 0.12 to 0.22 MHz by fitting a single spectrum composed of four scans to the lineshape model. It is limited by the linewidth and the SNR, which is attributed to the laser intensity noise ($<5\%$), the fluctuations of the atomic beam, the laser beam pointing vibration, and the electronic noise. For the long-term drift, a day-to-day stability has been tested using the D line. As shown in Fig. 4, the standard error of the mean was found to be 0.18 MHz, which is similar to

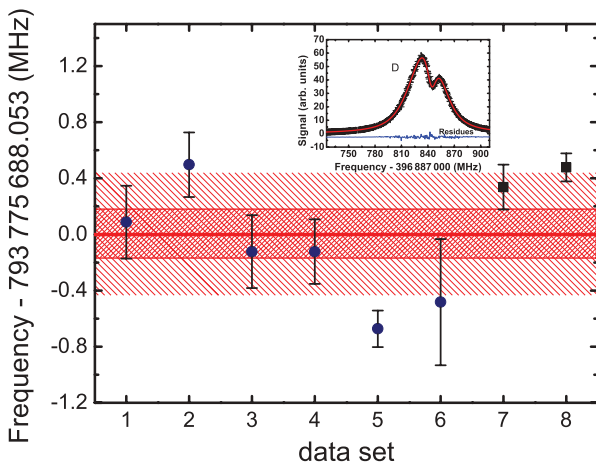


FIG. 4. (Color online) The distribution of the measured D -line absolute frequency. Two shaded areas indicate the regions of the standard error of the mean (± 0.18 MHz) and the 1σ standard deviation (± 0.45 MHz) of the distribution. The solid black bullet points are the measurements with good perpendicularity, and the solid black square points are with large deviations from the perpendicular position (see text). The inset shows a typical lineshape of the solid black square points.

the uncertainty given by a single spectrum statistic. For all the transition lines, the final statistical uncertainties are given to be 0.22 MHz.

The systematic errors are mostly contributed by the residual first-order Doppler shift. Ideally, the saturation spectroscopy with collinear laser beams interacting with an atomic beam would strongly suppress such a shift for the saturated dip, which resulted from the atoms with zero transverse velocity. However, in an atomic beam experiment, in order to measure a frequency to a high precision, two systematic effects must be carefully examined: the collinearity between the pump and the probe beams, and the perpendicularity between the lasers and the atomic beam.

The collinearity is estimated to be better than 0.43 mrad. This angle corresponds to a 0.5-mm separation of the pump and probe laser beams positioned 600 mm from the interaction area, which causes a shift of 270 kHz. This uncertainty estimation is limited by the visibility of two divergent UV laser beams in a far distance.

In a single laser beam excitation experiment, the nonperpendicular intersection of the laser and the atomic beam results in a shift of center frequency, owing to the first-order Doppler effect. In our experiment, this problem is resolved using a pair of counterpropagating beams (pump and probe). It is known that the nonperpendicularity will not affect the position of the Lamb dip, only the fluorescence background. However, the relative shift between the dip and the background [$\omega_{\text{shift}} \neq 0$ (see Sec II C)], as shown in the inset of Fig. 4, will induce a strong asymmetry in the spectrum profile, and could still possibly shift the fitted center frequency. In order to examine such an effect, the laser beams were purposely adjusted to be largely deviated from the perpendicular intersection with the atomic beam. A large angle between lasers and atomic beam was set to be $\Delta\phi \sim 20$ mrad, and enlarged the ω_{shift} to ~ 6 MHz (the inset of Fig. 4). We have found that, even in such an extreme condition, the center frequencies ω_0 of these misaligned measurements (solid black squares in Fig. 4) are still in agreement with the nominal measurements, within 1σ deviation of the measurements with careful alignment to the perpendicularity. These measurements demonstrate the Doppler-free feature of the saturated dip.

The second-order Doppler shift for the thermal atomic beam with a velocity of 243 m/s is only 0.3 kHz. The light shifts (ac Stark shifts) are negligible in our experiment because there is no energy level, which is linked to the relevant states ($6P_{1/2}$ and $7S_{1/2}$) to introduce a substantial perturbation by the 378-nm excitation laser. As for the Zeeman effect, while the laser is linearly polarized in the direction perpendicular to the 0.5-G Earth's magnetic field and the atomic beam, it mainly broadens the linewidth rather than shifts the line center. However, due to the finite extinction ratio of the polarizer, the shift is estimated to be <5 kHz. With a gate time of 0.1 s, the uncertainty due to OFC is ~ 20 kHz, as discussed in Ref. [23].

C. Absolute transition frequencies

The absolute transition frequencies are obtained by measuring the fundamental infrared 755-nm laser. For each data point, three frequencies (f_{rep} , f_o , f_{beat}) are directly measured

TABLE II. The transition frequencies of $6P_{1/2}(F) \rightarrow 7S_{1/2}(F')$. The cg (center of gravity) value is compared to that obtained in the previous work.

Line	$F - F'$	Laser frequency (MHz)
A	$^{203}\text{Tl}, 1 - 0$	793 761 871.36(35)
B	$^{205}\text{Tl}, 1 - 0$	793 763 391.29(35)
C	$^{203}\text{Tl}, 1 - 1$	793 774 051.26(35)
D	$^{205}\text{Tl}, 1 - 1$	793 775 688.05(35)
E	$^{203}\text{Tl}, 0 - 1$	793 795 156.48(35)
F	$^{205}\text{Tl}, 0 - 1$	793 796 997.62(35)
cg (of ^{205}Tl)		
This work	$6P_{1/2} \rightarrow 7S_{1/2}$	793 777.941(1) (GHz)
Experiment [28]	$6P_{1/2} \rightarrow 7S_{1/2}$	793 775.6 (GHz)
Theory [5]	$6P_{1/2} \rightarrow 7S_{1/2}$	793 101 (GHz)

using counters, and recorded in the data acquisition computer. The absolute frequency is then calculated using the following equation:

$$f_{\text{measure}} = N \times f_{\text{rep}} \pm f_o \pm f_{\text{beat}},$$

where the repetition rate of comb laser f_{rep} is ~ 1 GHz, the offset frequency of comb laser f_o and the beat frequency f_{beat} are typically several hundreds MHz. The \pm signs and the N (a large integer, $\sim 4 \times 10^5$ for 755 nm) are first inferred from the wavelength measurements of a 0.5-GHz accuracy wavemeter and then confirmed using the method described in Ref. [23].

The final absolute frequencies of all six components of the thallium $6P_{1/2} \rightarrow 7S_{1/2}$ transition, including three hyperfine transitions of two isotopes, are listed in Table II. They are labeled as A–F for identification, and in comparison with the previous experimental measurements and the theoretical calculations. The center-of-gravity value of ^{205}Tl calculated from the absolute frequency is also listed to be compared with the previous determination of [5,28]. In theory [5], the Coulomb-Gaunt transition energy is $26\,455\text{ cm}^{-1}$, corresponding to 793 101 GHz.

D. HFS, IS, and the mean-square isotopic change $\lambda_{c,m}$

For both the $6P_{1/2}$ ground state and the $7S_{1/2}$ excited state, their hyperfine constants (HFA) can be deduced from our measurements as listed in Table III. The accuracy of our results

TABLE III. Summary of measurements of thallium $6P_{1/2}$ and $7S_{1/2}$ hyperfine constants A and isotope shift (IS) for two stable isotopes. The previous experimental results and theoretical calculations are listed for comparison. All results are in MHz.

	$6P_{1/2} \text{ } ^{205}\text{Tl}$	$6P_{1/2} \text{ } ^{203}\text{Tl}$	$7S_{1/2} \text{ } ^{205}\text{Tl}$	$7S_{1/2} \text{ } ^{203}\text{Tl}$	IS of $6P_{1/2} \rightarrow 7S_{1/2}$
This work	21 310.24(70)	21 105.22(70)	12 296.09(70)	12 179.90(70)	1658.33(70)
Reference [12]			12 294.5(15)	12 180.5(18)	1659.0(6)
Reference [13]			12 297.2(16)	12 181.6(22)	
Reference [29]			12 284.0(60)	12 172.0(60)	
Reference [30]			12 318(36)	12 225(42)	
Reference [31]	21 310.835(5)	21 105.447(5)			
Theory [10]	21 390		12 596		
Theory [5]	21 663		12 666		
Theory [32]	21 300		12 760		
Theory [33]	21 623		12 307		

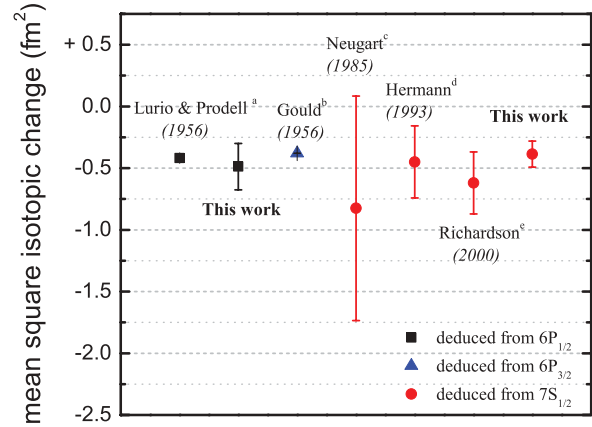


FIG. 5. (Color online) Comparison of the mean-square isotopic change $\lambda_{c,m}$ based on various experimental results. $\lambda_{c,m}$ values shown in the figure were extracted by combining theoretical and experimental values. The value $\Delta/\lambda_{c,m} = -2.48 \times 10^{-4} \text{ fm}^2$ for $6P_{1/2}$, $43.0 \times 10^{-4} \text{ fm}^2$ for $6P_{3/2}$, and $-7.62 \times 10^{-4} \text{ fm}^2$ for $7S_{1/2}$ were theoretically calculated by [32]. We infer $\lambda_{c,m} = -0.386(94) \text{ fm}^2$ in this work. These parameters inferred from the results of the $6P_{1/2}$, $6P_{3/2}$, and $7S_{1/2}$ states HFS are shown here. ^aRef. [31], $\lambda_{c,m} = -0.418(1) \text{ fm}^2$ of $6P_{1/2}$; ^bRef. [34], $\lambda_{c,m} = -0.379(2) \text{ fm}^2$ of $6P_{3/2}$; ^cRef. [29], $\lambda_{c,m} = -0.825(910) \text{ fm}^2$ of $7S_{1/2}$; ^dRef. [13], $\lambda_{c,m} = -0.450(292) \text{ fm}^2$ of $7S_{1/2}$; ^eRef. [12], $\lambda_{c,m} = -0.620(251) \text{ fm}^2$ of $7S_{1/2}$.

is ~ 700 kHz. For the $6P_{1/2}$ ground-state HFA, our results are in good agreement with the previous measurements using microwave techniques [31]. But, for the $7S_{1/2}$ excited-state HFA, our error is about a factor of 2 smaller than the value from the previous result in Ref. [12].

The isotope shift (IS) of the $6P_{1/2} \rightarrow 7S_{1/2}$ of the two naturally occurring isotopes of thallium, ^{205}Tl (70.5%) and ^{203}Tl (29.5%), was also derived from our measurements. The result obtained is in good agreement with [12], which employed a gas cell and an optical reference cavity, with comparable accuracies.

The mean-square isotopic change $\lambda_{c,m}$ between ^{205}Tl and ^{203}Tl , which is sensitive to both the radial distribution of the neutron magnetization and charge distributions in the isotopes, can be deduced from our results by calculating the hyperfine anomalies of the $6P_{1/2}$ and $7S_{1/2}$ states. Both measurements

should give the same value of the isotopic change. The hyperfine anomaly is written as $\Delta = [(A^{205}/A^{203})(\mu_I^{203}/\mu_I^{205}) - 1]$, where the HFAs A^{205} and A^{203} can be found in Table III. Using the known ratio between the nuclear magnetic moments $\mu_I(^{205}\text{Tl})/\mu_I(^{203}\text{Tl}) = 1.009\,836\,13(6)$ measured in Ref. [35], $\Delta_{7S_{1/2}} = -2.94(81) \times 10^{-4}$ and $\Delta_{6P_{1/2}} = -1.21(47) \times 10^{-4}$ are resulted. To infer the mean-square isotopic change, the ratios of $\Delta/\lambda_{c,m}$ of the atomic thallium have been theoretically calculated by [32], which gave $\Delta/\lambda_{c,m} = -7.62 \times 10^{-4}\text{fm}^2$ for $7S_{1/2}$, and $-2.48 \times 10^{-4}\text{fm}^2$ for $6P_{1/2}$. Therefore,

$$\lambda_{c,m} = -0.39(11) \text{ fm}^2(7S_{1/2}),$$

$$\lambda_{c,m} = -0.49(19) \text{ fm}^2(6P_{1/2}).$$

Figure 5 shows the comparison of the mean square isotopic changes $\lambda_{c,m}$ based on various experimental results. Among the experiments based on the $7S_{1/2}$ state, our result gives the most precise value and is in very good agreement with the results deduced from the most accurate values based on $6P_{1/2}$ and $6P_{3/2}$ states measured using microwave techniques [31,34]. Meanwhile, the value deduced from our $6P_{1/2}$ state measurement is consistent with our own $7S_{1/2}$ state measurements and in agreement with the others.

IV. CONCLUSION

In summary, the atomic thallium $6P_{1/2} \rightarrow 7S_{1/2}$ saturation spectrum was measured using a tunable 378-nm SHG laser exciting a collimated atomic beam with frequency calibration against an optical frequency comb. The center frequencies are precisely determined by fitting the spectrum to a theoretical

model. By the application of the saturation technique, we are able to reduce one of the main systematic errors in the conventional atomic beam setup, the first-order Doppler effect, to a level of sub-MHz.

The absolute frequencies of all hyperfine components in the $6P_{1/2} \rightarrow 7S_{1/2}$ transition of stable thallium isotopes (^{205}Tl and ^{203}Tl) have been measured with an accuracy of 350 kHz. The HFS and IS of $6P_{1/2}$ and $7S_{1/2}$ obtained from our results are with a 0.7-MHz accuracy. They are in agreement with previous measurements. These results should provide one of the few handles on the neutron radial distribution in nuclei and calibration for nuclear structure calculations which are of importance to the understanding of PNC and QED effects in thallium and heavier atoms [5,32,36].

In particular, the values of HFS within the $7S_{1/2}$ transition are a factor of 2 better than previous results from the precision of MHz to sub-MHz. This can advance the understanding of the nuclear magnetization distribution, which is hardly accessible to be measured independently [37]. In addition, the mean-square isotopic change $\lambda_{c,m}$ deduced from the hyperfine anomalies of the $7S_{1/2}$ state has also been improved and is in very good agreement with the most precise value deduced from the hyperfine anomaly of $6P_{1/2}$.

ACKNOWLEDGMENTS

We thank S.-M. Yang and W.-L. Cheng for their contributions in the initial development of the experiment setup. This work was supported by the National Science Council of Taiwan under Grants No.100-2112-M-007-006-MY3 and No. 99-2112-M-007-001-MY3.

-
- [1] C. S. Wood, S. C. Bennett, D. Cho, B. P. Masterson, J. L. Roberts, C. E. Tanner, and C. E. Wieman, *Science* **275**, 1759 (1997).
 - [2] V. A. Dzuba, V. V. Flambaum, and J. S. M. Ginges, *Phys. Rev. D* **66**, 076013 (2002).
 - [3] P. A. Vetter, D. M. Meekhof, P. K. Majumder, S. K. Lamoreaux, and E. N. Fortson, *Phys. Rev. Lett.* **74**, 2658 (1995).
 - [4] N. H. Edwards, S. J. Phipp, P. E. G. Baird, and S. Nakayama, *Phys. Rev. Lett.* **74**, 2654 (1995).
 - [5] M. G. Kozlov, S. G. Porsev, and W. R. Johnson, *Phys. Rev. A* **64**, 052107 (2001).
 - [6] V. A. Dzuba, V. V. Flambaum, and M. S. Safronova, *Phys. Rev. A* **73**, 022112 (2006).
 - [7] J. Ginges and V. V. Flambaum, *Phys. Rep.* **397**, 63 (2004).
 - [8] V. A. Dzuba, V. V. Flambaum, and M. G. Kozlov, *Phys. Rev. A* **54**, 3948 (1996).
 - [9] M. S. Safronova, *Can. J. Phys.* **89**, 371 (2011).
 - [10] U. I. Safronova, M. S. Safronova, and W. R. Johnson, *Phys. Rev. A* **71**, 052506 (2005).
 - [11] I. Fan, T.-L. Chen, Y.-S. Liu, Y.-H. Lien, J.-T. Shy, and Y.-W. Liu, *Phys. Rev. A* **84**, 042504 (2011).
 - [12] D. S. Richardson, R. N. Lyman, and P. K. Majumder, *Phys. Rev. A* **62**, 012510 (2000).
 - [13] G. Hermann, G. Lasnitschka, and D. Spengler, *Z. Phys. D* **28**, 127 (1993).
 - [14] W. Demtroder, *Laser Spectroscopy: Basic Concepts and Instrumentation*, 3rd ed. (Springer, New York, 2003).
 - [15] C. M. Klimcak and J. C. Camparo, *Phys. Rev. A* **30**, 1791 (1984).
 - [16] B. M. Tissue and B. L. Fearey, *J. Opt. Soc. Am. B* **11**, 542 (1994).
 - [17] J. W. Daily, *Appl. Opt.* **17**, 225 (1978).
 - [18] D. Budker and D. Kimball, *Atomic Physics: An Exploration through Problems and Solutions*, 2nd ed. (Oxford University Press, Oxford, UK, 2004), p. 154.
 - [19] V. Gerginov, C. E. Tanner, S. Diddams, A. Bartels, and L. Hollberg, *Phys. Rev. A* **70**, 042505 (2004).
 - [20] D. Das and V. Natarajan, *Phys. Rev. A* **75**, 052508 (2007).
 - [21] J. Friebe, A. Pape, M. Riedmann, K. Moldenhauer, T. Mehlstäubler, N. Rehbein, C. Lisdat, E. M. Rasel, W. Ertmer, H. Schnatz, B. Lipphardt, and G. Grosche, *Phys. Rev. A* **78**, 033830 (2008).
 - [22] E. J. Salumbides, V. Maslinskas, I. M. Dildar, A. L. Wolf, E.-J. van Duijn, K. S. E. Eikema, and W. Ubachs, *Phys. Rev. A* **83**, 012502 (2011).
 - [23] Y.-H. Lien, K.-J. Lo, H.-C. Chen, J.-R. Chen, J.-Y. Tian, J.-T. Shy, and Y.-W. Liu, *Phys. Rev. A* **84**, 042511 (2011).
 - [24] V. Gerginov, K. Calkins, C. E. Tanner, J. J. McFerran, S. Diddams, A. Bartels, and L. Hollberg, *Phys. Rev. A* **73**, 032504 (2006).

- [25] M. Harris, E. L. Lewis, D. McHugh, and I. Shannon, *J. Phys. B: At. Mol. Phys.* **17**, L661 (1984).
- [26] M. G. Prentiss and S. Ezekiel, *Phys. Rev. Lett.* **56**, 46 (1986).
- [27] H. Flores-Llomas, *J. Appl. Crystallogr.* **34**, 136 (2001).
- [28] R. L. Kurucz, Atomic spectral line database, <http://www.pmp.uni-hannover.de/cgi-bin/ssi/test/kurucz/sekur.html>.
- [29] R. Neugart, H. H. Stroke, S. A. Ahmad, H. T. Duong, H. L. Ravn, and K. Wendt, *Phys. Rev. Lett.* **55**, 1559 (1985).
- [30] C. Schuler, M. Ciftan, L. B. III, and H. Stroke, *J. Opt. Soc. America* **52**, 501 (1962).
- [31] A. Lurio and A. G. Prodel, *Phys. Rev.* **101**, 79 (1956).
- [32] A.-M. Mårtensson-Pendrill, *Phys. Rev. Lett.* **74**, 2184 (1995).
- [33] V. A. Dzuba, V. V. Flambaum, M. G. Kozlov, and S. G. Porsev, *Zh. E'ksp. Teor. Fiz.* **114**, 1636 (1998) [*Sov. Phys.-JETP* **87**, 885 (1998)].
- [34] G. Gould, *Phys. Rev.* **101**, 1828 (1956).
- [35] E. B. Baker and L. W. Burd, *Rev. Sci. Instrum.* **34**, 238 (1963).
- [36] J. S. Grossman, L. A. Orozco, M. R. Pearson, J. E. Simsarian, G. D. Sprouse, and W. Z. Zhao, *Phys. Rev. Lett.* **83**, 935 (1999).
- [37] A. E. Barzakh, L. K. Batist, D. V. Fedorov, V. S. Ivanov, K. A. Mezilev, P. L. Molkanov, F. V. Moroz, S. Y. Orlov, V. N. Panteleev, and Y. M. Volkov, *Phys. Rev. C* **86**, 014311 (2012).